Weak response of oceanic dimethylsulfide to upper mixing shoaling induced by global warming

S. M. Vallina[†‡§], R. Simó[†], and M. Manizza[‡¶∥]

[†]Institut de Ciències del Mar–Consejo Superior de Investigaciones Cientificas, 08003 Barcelona, Spain; [‡]School of Environmental Sciences, University of East Anglia, Norwich NR4 7TJ, United Kingdom; [¶]Max-Planck-Institut für Biogeochemie, 07745 Jena, Germany; and [∥]Department of Earth, Atmospheric, and Planetary Sciences, Massachusetts Institute of Technology, Cambridge, MA 02139

The solar radiation dose in the oceanic upper mixed layer (SRD) has recently been identified as the main climatic force driving global dimethylsulfide (DMS) dynamics and seasonality. Because DMS is suggested to exert a cooling effect on the earth radiative budget through its involvement in the formation and optical properties of tropospheric clouds over the ocean, a positive relationship between DMS and the SRD supports the occurrence of a negative feedback between the oceanic biosphere and climate, as postulated 20 years ago. Such a natural feedback might partly counteract anthropogenic global warming through a shoaling of the mixed layer depth (MLD) and a consequent increase of the SRD and DMS concentrations and emission. By applying two globally derived DMS diagnostic models to global fields of MLD and chlorophyll simulated with an Ocean General Circulation Model coupled to a biogeochemistry model for a 50% increase of atmospheric CO_2 and an unperturbed control run, we have estimated the response of the DMS-producing pelagic ocean to global warming. Our results show a net global increase in surface DMS concentrations, especially in summer. This increase, however, is so weak (globally 1.2%) that it can hardly be relevant as compared with the radiative forcing of the increase of greenhouse gases. This contrasts with the seasonal variability of DMS (1000–2000% summer-to-winter ratio). We suggest that the ''plankton–DMS–clouds–earth albedo feedback'' hypothesis is less strong a long-term thermostatic system than a seasonal mechanism that contributes to regulate the solar radiation doses reaching the earth's biosphere.

mixed layer depth | solar radiation dose | global modeling

Ocean-emitted dimethylsulfide (DMS) has been suggested to play a climatic role by contributing to cloud droplet condensation and thereby to cloud albedo. As such a climate-active compound, DMS was proposed as a candidate to partially counteract human-induced global warming (GW) through a global biogeochemical feedback between oceanic biosphere and climate, the so-called "CLAW hypothesis" (1). To quantitatively assess the feasibility and magnitude of this potential long-term climate-stabilizing response, it is important to understand which are the main factors that drive DMS dynamics: if we can estimate how they are changing due to GW, we should be able to predict the DMS response. Early works pointed to the mutual interaction of several factors (i.e., phytoplankton community structure, zooplankton grazing, bacterial activity, etc.), over which the mixed layer depth (MLD) seems to have some kind of regulatory influence (2, 3). However, more recent studies have strongly suggested that solar radiation is the key factor regarding DMS dynamics, notably through its stress effects on phytoplankton and inhibitory effects on heterotrophic bacterioplankton (4–8). One suggestion is that the enzymatic cleavage of dimethylsulfoniopropionate (DMSP) into DMS in phytoplankton is part of an antioxidant system that protects the cell from endogenous, hazardous hydroxyl (OH) radicals under high-light stressing conditions (5). This hypothesis is supported by several laboratory studies (5, 6, 9, 10) as well as local and global time series analyses (7, 11, 12, 47).

In this context, phytoplankton is a necessary, but not sufficient, condition for the production of DMS. It is obvious that some phytoplankton activity needs to be present, but phytoplankton biomass proxies like chlorophyll-a (CHL) are not correlated with DMS concentrations over large scales except for at high latitudes (13) and in highly productive near-coastal regions (3). In these (usually nutrient-replete) regions, the solar radiation dose in the upper mixed layer (UML) drives both phytoplankton biomass and DMS concentrations. These have been postulated to be the "DMS bloom-regime" regions (7). However, in subtropical and low temperate regions (which cover most of the ocean's surface), DMS is basically driven by the solar radiation dose, both increasing in summer despite CHL reduction due to nutrient depletion after water column stratification. These have been postulated to be the "DMS stress-regime" regions (7). Therefore, with the exception of high levels of DMS resulting from some phytoplankton blooms, most of the DMS dynamics could be predicted based purely on geophysical data (3, 7). In support of that, recent works have found that the daily averaged solar radiation dose received in the UML (hereafter SRD) seems to be the key factor governing DMS dynamics at all spatial scales, from the local to the global (11, 12). These results also explain why previous diagnostic models of DMS concentrations, based basically (3) or exclusively (14) on the MLD, work so well: the MLD might simply be a proxy of the SRD. Because MLD seasonality is related to surface irradiance (an increase on surface irradiance is usually followed by a decrease in the MLD), a multiplicative (nonlinear) effect arises on the SRD. This leads to the observed nonlinearity of the relationship between DMS and MLD, whereas DMS is linearly related to SRD.

MLD is predicted to be reduced by several meters in most regions of the ocean as a consequence of GW, because the increase in air temperature would increase the atmosphere-to-ocean heat flux (then reinforcing water column stratification) (15). In this regard, it has been speculated that, because of the links between MLD, SRD, and DMS, in a GW scenario, the shoaling of ocean stratification will imply an increase of DMS concentrations and its fluxes to the atmosphere (3, 7), in support of the CLAW hypothesis. Because DMS is believed to be the main contributor to cloud condensation nuclei (CCN) concentrations over marine remote regions (12, 16–22) and CCN numbers are related to cloud formation, cloud optical properties, and lifetime [hence to the earth

albedo (1)], the anticipated DMS increase might constitute a natural negative feedback mechanism that could counteract the effects of GW on earth's climate (1, 23). The present study seeks to estimate this (potential) DMS increase under GW conditions by using the global relationship between DMS concentrations and the SRD (11) as a diagnostic model, as well as the diagnostic model proposed by Simó and Dachs (3), that relates DMS to the MLD and CHL. Both diagnostic models are applied to global model outputs of MLD (from which the SRD is calculated) and CHL for the year 2061, obtained under a 50% increase in CO_2. A control with today's levels of CO_2 is run as a reference. The results are discussed in the context of the CLAW hypothesis.

Results and Discussion

With the aim at quantifying the (potential) future "MLD reduction–SRD increase–DMS increase," we applied the globally derived DMS diagnostic equations of Vallina and Simó (11) (SRD-model; see Eq. **2** in *Data and Methodology*) and Simó and Dachs (3) (MLD-model; see Eqs. **3** and **4** in *Data and Methodology*) to modeled global fields of MLD and CHL obtained for 2061 (15) under two scenarios (GW vs. Control; see *Control and Global Warming Scenarios* in *Data and Methodology*).

Global Validity of the DMS Diagnostic Models. To evaluate the validity of the DMS diagnostic models used, we compared their results against actual data. Fig. 1 shows the Hovmoller Diagrams (*Top* and *Middle*) obtained both from data [Global Sea Surface (GSS)–DMS database and Kettle and Andreae (24)] as well as from model results (see Fig. 1 legend), along with the global maps of seasonal correlations (13) between DMS modeled results from the control run against the Kettle and Andreae (24) climatology (Fig. 1 *Bottom*). In general, there is good agreement between DMS data and model estimates. However, for the control run, the SRD-model is unable of capturing the highest 10% zonally averaged DMS values ($\gtrsim$4 nM), whereas the MLD-model, because it includes the bloom-regimes, cannot capture only the highest 4% zonally averaged DMS data values ($\gtrsim$6 nM). The correlation maps show that, with the exception of the equatorial regions (where there is almost no seasonality in the variables), the seasonality of the DMS data is very well captured by both models virtually all over the global ocean. A scatter-plot analysis between the zonally averaged DMS values from model against data [see supporting information (SI) Fig. 6] confirms their global validity (i.e., Spearman correlation coefficients of $\approx$0.8 between MLD-model and SRD-model for the control run vs. Kettle and Andreae (24); see SI Fig. 6 *AA1* and *BB2*).

DMS Estimates Under Global Warming. Fig. 2 shows the global maps of estimated surface DMS concentration fields under GW conditions for the three time periods considered, obtained with both diagnostic models. The results are fairly similar, yet some differences can be observed. Although both models display a clear seasonal pattern of higher DMS during each hemispheric summer, this seasonality is more marked in the SRD-model: $DMS^{GW}_{SRD-model}$ concentrations are slightly higher than $DMS^{GW}_{MLD-model}$ in each hemispheric summer, and vice versa for each hemispheric winter. On the other hand, the MLD-model gives higher DMS concentrations at high latitudes due to algal blooms.

DMS Increase Under Global Warming. Figs. 3 and 4 show the global maps of the estimated increases of DMS under GW with both models. First, we notice that, although in some regions DMS decreases, there is a general increase of DMS concentrations over most of the globe. However, these increases are generally very weak, both in absolute change and in percentage of change. For example, in the case of the MLD-model, the 95% percentile from the annual maps is +0.13 nM for the absolute change and + 6.3% for the percentage of change (the 5% percentile is −0.08 nM and −3.22%, respectively). In the case of the SRD-model, these values are even
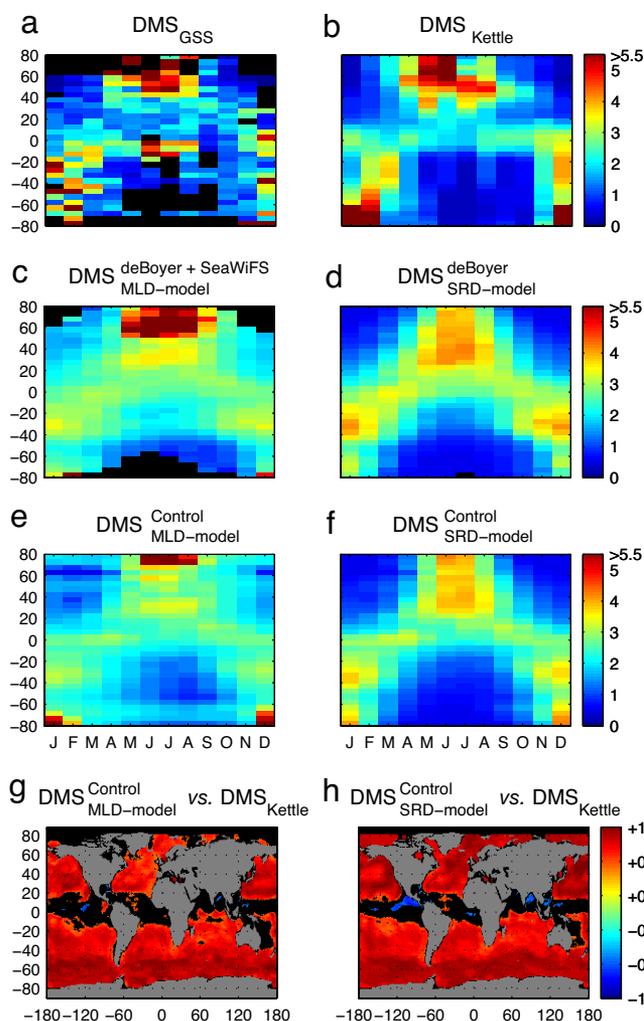
Fig. 1. Global DMS (nM) distributions. (*a–f*) Shown are the Hovmoller Diagrams for GSS data (*a*), Kettle and Andreae (24) climatology (*b*), present-day MLD-model (MLD from ref. 45) with CHL from a SeaWiFS 2002–2004 climatology) (*c*), present-day SRD-model (MLD from ref. 45) (*d*), MLD-model (MLD and CHL from control run) (*e*), and SRD-model (MLD from control run) (*f*). The colorbar palette has been cut at 5.5 nM (corresponding to the 95% percentile of zonally averaged DMS GSS data) for the sake of visual comparison of modeled results against data. The GSS raw data ($\approx$33,000 points) were gridded into a 180° × 360° × 12 (latitude, longitude, month) array climatology ($\approx$5,700 points) before making the diagram. (*g* and *h*) Shown are the global maps of seasonal correlation (13) between modeled DMS results from the control run in an MLD-model (*g*) and an SRD-model (*h*) against the Kettle and Andreae (24) climatology. Only significant (95%) values are shown.

lower: the 95% percentiles are +0.09 nM and +4.2% (the 5% percentiles are −0.03 nM and −1.34%). Interestingly, both models show three regions where the DMS increase is the highest: the North Atlantic between 40°N and 60°N, some zones of the equatorial Pacific, and the Southern Ocean. Overall, these results are an indication that an increase of DMS under GW scenario due to a net reduction of the MLD seems possible and robust, but that the global strength of such response will probably be very weak. It is worth noting, however, that the predicted DMS response in tropical regions, and particularly next to the Maritime Continent, Asian equatorial Pacific (where the predicted annual increase is of the order of 10–15%), can be climatically important. This region is weakly affected by anthropogenic sulfur emissions, receives large incident solar radiation, and plays an important role in energy distribution through convection and atmospheric teleconnections

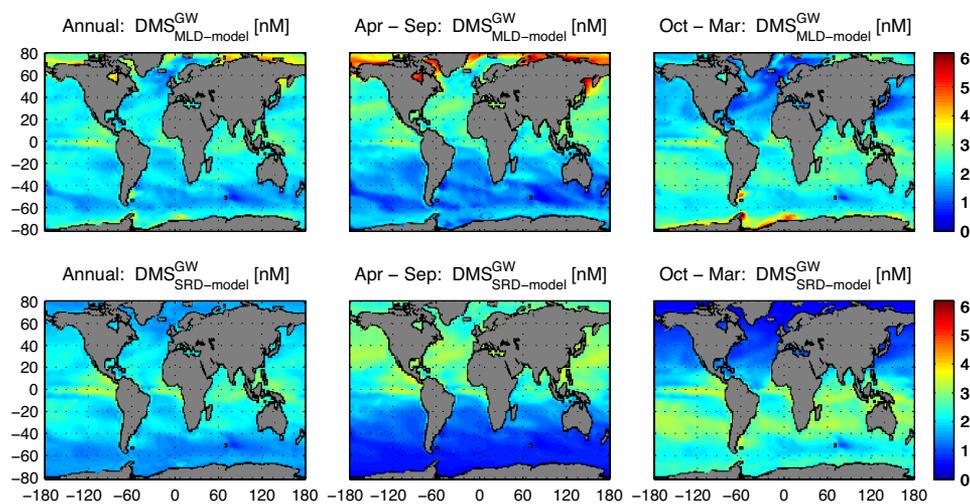**Fig. 2.** Simulated fields of surface DMS concentrations under GW conditions from the MLD-model (*Upper*) (3) and the SRD-model (*Lower*) (11) for three time periods: annual average (*Left*), April–September average (*Center*), and October–March average (*Right*).

(25, 26). Changes in the radiative balance of this region might have ample climate implications.

A more detailed analysis reveals that the results obtained from the two diagnostic models differ markedly in the seasonality. Whereas for the MLD-model the DMS increases are approximately equally distributed in the two time periods (April–September and October–March), the SRD-model predicts higher DMS increases in each hemispheric summer. This is important because the efficiency at which DMS is oxidized to sulfates is highly dependent on the concentration of atmospheric OH radicals (27). Because OH production is UV dependent, it displays a clear seasonality with higher values during each hemispheric summer (28). Although DMS conversion into CCN also is influenced by nitrate radical DMS oxidation at nighttime (29) and by the presence of other aerosols, particularly over polluted regions, the central role of OH suggests that any coupling (or mismatch) between the seasonalities of DMS and OH could amplify (or buffer) the seasonal contribution of biogenic sulfur to CCN production.

Further, for DMS-derived CCN to become more effective in cooling the earth, their increase of the cloud optical depth should co-occur with the highest solar irradiances (i.e., in each hemispheric summer). This is particularly true at high latitudes where the summer-to-winter ratio of solar incident radiation is higher. Over

these regions, an increase of DMS during winter would be of little help regarding earth cooling, because of low OH to oxidize DMS into CCN and low solar radiation to reflect back to the space. In other words, estimating the annual changes in DMS concentrations due to GW without giving information about the season when these changes are predicted to occur results in an incomplete picture if we are to interpret our results within the context of the CLAW hypothesis.

To better quantify this difference, we calculated the globally averaged (not spatially resolved) percentage of DMS change, which takes into account the area of each pixel, for three cases: annually, summer conditions, and winter conditions. Results from the two diagnostic models are shown in Fig. 5. We can clearly observe how, although the annual average is almost identical for the two models ($\approx$1.2%), the summer-to-winter ratio is higher for the SRD-model ($\approx$0.8% in winter, $\approx$1.8% in summer) than for the MLD-model ($\approx$1.1% in winter, $\approx$1.5% in summer). As we stated previously, in the context of DMS predictions by empirical diagnostic models the MLD can be regarded as a proxy of the SRD (11), so, in principle, the results using one or the other should have been rather similar. Why, therefore, are there such important differences in the seasonality of the change? The seasonality of the MLD can be used indeed as a good (nonlinear) proxy of the seasonality of
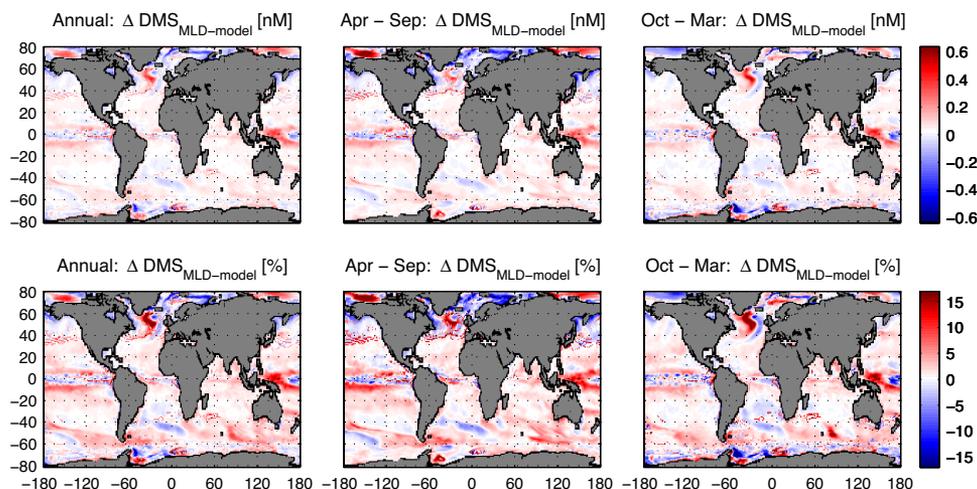

Fig. 3. Global maps of the estimated change of DMS under GW obtained with the MLD-model (3). (*Upper*) Averaged absolute change. (*Lower*) Percentage of change.

Fig. 4. Global maps of the estimated change of DMS under GW obtained with the SRD-model (11). (*Upper*) Averaged absolute change. (*Lower*) Percentage of change.

SRD because, over seasonal scales, the MLD is mostly set by surface irradiance, and both concur to set the SRD. However, this is not necessarily the case over the time scale of GW. For example, a wintertime reduction of the MLD at a high-latitude region (e.g., the Southern Ocean) due to GW would hardly cause a significant increase of the regional SRD because the surface irradiance is too low. Therefore, if the driving force of the oceanic DMS production is the SRD, using simply an MLD model may overpredict the DMS increase in this scenario. This especially would be the case when estimating wintertime increases due to GW over high-latitude regions.

Nevertheless, despite these differences, both models are fairly consistent in their predictions. On a global annual average, the DMS percentage of increase is $\approx 1.2\%$; in the summer conditions it could go up to 1.8% (Fig. 5). Our results are consistent with other estimates of the oceanic DMS response to GW. Bopp *et al.* (30), based on a completely different diagnostic equation to estimate surface DMS, reported a global increase of DMS flux of 3% in a scenario of 100% increase of CO_2 (from ≈ 350 ppm in 1990 to ≈ 700 ppm by 2060). This DMS increase was calculated to give a global radiative forcing of -0.05 W m^{-2}, i.e., $\approx 2\%$ reduction of the estimated positive radiative forcing due to increased CO_2 (approximately $+3$ W m^{-2}) (30). Based on a mechanistic ecosystem-DMS model, Gabric *et al.* (46) predicted a 5% increase of DMS flux for a region of the Southern Ocean under a GW scenario caused by a CO_2 tripling (by 2080) relative to preindustrial levels. They esti-

mated the associated radiative forcing to be -0.3 W m^{-2}, i.e., an $\approx 4\%$ reduction of the estimated CO_2 radiative forcing (approximately $+7$ W m^{-2}). Interestingly Gabric *et al.* (31) also made use of the Simó and Dachs (3) MLD-model to estimate a global DMS increase under GW based on MLD fields simulated by the Commonwealth Scientific and Industrial Research Organisation (CSIRO) Ocean General Circulation Model (OGCM) and CHL fields predicted with an ecological model of their own. They estimated a global DMS flux increase of 14%. This value, however, was highly influenced by an austral-spring DMS flux increase in the 50–60°S region of $\approx 1000\%$. Out of this season or for any period of the year at the remaining latitudes, the DMS flux shows either a slight increase or a slight decrease (31). The way they modeled CHL was substantially different from our model, and this may account for the discrepancy in the results. Their ecosystem model was applied in a zero-dimensional (0D) mode by 10° latitudinal bands, with recalibration for each one of them. Our approach is based on a global 3D coupled physical–ecological model.

DMS and the CLAW Hypothesis. When Charlson *et al.* (1) proposed the CLAW hypothesis, they postulated a global climate feedback mechanism that regulates either temperature and/or solar irradiance. However, at that time, they were not able yet to define the nature and tempo of the processes that drive DMS variability, so they associated DMS dynamics with long-term climate evolution (1, 32). But temperature and irradiance, although tightly linked, are not the same thing. Twenty years later, it starts to become clear that DMS increases with incident light (5, 7, 10, 11) but not with temperature (11, 33). Further, surface DMS concentrations are highly seasonal, as CCN production is (12, 13). For DMS to be oxidized to sulfates and produce biogenic CCN, high levels of atmospheric OH radicals are needed (32). Because OH is mainly driven by UV radiation, DMS and OH are usually in phase with maxima in summer (12). This represents an efficient seasonal mechanism for enhanced biogenic CCN formation at the time when harmful solar radiation is the highest.

On the other hand, the DMS-feedback capability as a global thermal regulator over longer time-scales such as that of GW seems to be weak: the same mechanisms that produce 1000–2000% seasonal increases of DMS concentrations (7, 11) (Fig. 2) are able to produce only a weak response to GW conditions (1.2%; Figs. 3–5). Also, the radiative forcing of a long-lived gas like CO_2 is very homogeneous both in time and space (30), whereas CCN formation from DMS and its influence on cloud properties is regional and seasonal because both atmospheric DMS and CCN have much

Fig. 5. Globally averaged percentage of DMS change under GW obtained from the MLD-model (3) and SRD-model (11) for three cases: annually, summer conditions, and winter conditions. Summer and winter conditions refer to the regions and periods with an daily averaged solar surface irradiance higher and lower than 200 W m^{-2}, respectively.

ENVIRONMENTAL SCIENCES

shorter lifetimes. Then a DMS-climate feedback would be most apparent over seasonal scale. There seems to be, therefore, a mismatch between the scales at which DMS influences climate and GW operates.

We therefore propose a revision of the point of view on the CLAW hypothesis: rather than looking at the DMS–CCN–cloud albedo feedback as a long-term mechanism contributing to regulate the earth's temperature, we should see it as a seasonal mechanism contributing to regulate the solar radiation dose received by the marine pelagic biosphere.

Conclusions

We have estimated the DMS increase under GW conditions (50% increase from current CO_2 levels) by means of two global empirically derived diagnostic DMS models for which the MLD is a critical parameter. The goal was to evaluate whether the predicted net reduction of the MLD in GW scenarios would trigger a significant DMS increase as proposed previously (2, 3, 7).

Our results point toward a net global increase in surface-ocean DMS concentrations, particularly during each hemispheric summer, when a derived increase in CCN numbers and cloud albedo would be more effective in cooling the earth because it is the period of higher incident solar radiation. This increase, however, is weak (globally of 1.2% and only in very few places it is higher than $\approx 5\%$), so it can hardly be of much relevance to counteract GW. This contrasts with the seasonal variability of DMS concentrations (easily 1000–2000%). Therefore we suggest that the "DMS–CCN–cloud albedo" feedback proposed by the CLAW hypothesis does not act as a significant longer-term thermostatic mechanism in the anthropogenically perturbed Holocene but rather as a seasonal earth system mechanism that contributes to regulate the solar radiation dose received by the oceanic pelagic biosphere. How much this seasonal mechanism has been contributing to the global radiative balance throughout the history of the preindustrial earth is still uncertain (32), but although a significant role is likely, it is not expected to change dramatically with the prospected manifestations of GW within the current century. However, mechanisms other than MLD changes also could be involved in a DMS feedback loop, such as changes in aeolian or riverine input of nutrients that could alter marine biology (and hence DMS production) in a GW scenario in ways that are not captured by the seasonality of the SRD dependence. To evaluate whether these effects could be of higher importance than those related to MLD changes, a fully coupled earth system model, including a reliable mechanistic characterization of the oceanic DMS cycle, is needed.

Data and Methodology

Model Data of the MLD and CHL. Global monthly fields of MLD are outputs from the ORCA-LIM, a global version of OPA (34). This is a three-dimensional (3D) Ocean General Circulation Model (OGCM) coupled to the LIM sea-ice model. OPA is based on primitive equations (35, 36) where the vertical eddy diffusivity and viscosity coefficients are calculated by a 1.5-order turbulent kinetic energy model (37). Subgrid eddy induced mixing is parameterized according to ref. 38. CHL is obtained from the coupling of PlankTOM5 to ORCA-LIM. PlakTOM5 is a biogeochemistry model based on Plankton Functional Types (PFT) (39). It includes phosphorous, silicate, iron, and light colimitation and represents five PFT: mixed-phytoplankton, diatoms and coccolithophores for phytoplankton, plus meso- and micro-size classes for zooplankton (39). CHL is the sum of the CHL of all three phytoplankton types.

Solar Radiation Dose. Monthly global maps of daily averaged solar radiation dose (W m^{-2}) in the UML (or SRD) are estimated assuming an exponential decay of the daily averaged surface solar irradiance (I_0) with depth (z):

$$SRD = I_{uml} = \frac{1}{MLD} \int_0^{MLD} I_0 \times \exp(-k \times z) dz$$

$$= \frac{I_0}{MLD \times k} \times (1 - \exp(-k \times MLD)). \quad [1]$$

I_0 is assumed to be 50% of the daily averaged solar irradiance at the top of the atmosphere (I_{toa} W m^{-2}) (40), which is calculated following Brock (41). We assume a general solar-radiation extinction coefficient (k) of 0.06 m^{-1}, which is a reasonable approximation for spectrum-centered wavelengths in open ocean waters (42).

DMS Diagnostic Models.

- SRD-model:

$$DMS = 0.492 + 0.019 \times SRD. \quad [2]$$

- MLD-model:

  if CHL/MLD ≥ 0.02:

$$DMS = 0.6 + 55.8 \times (CHL/MLD); \quad [3]$$

  if CHL/MLD < 0.02:

$$DMS = 5.7 - Ln(MLD). \quad [4]$$

Control and Global Warming Scenarios. We performed two parallel transient simulations (56 years, from 2005 to 2061) that differed in their atmospheric forcing ψ (air temperature, wind speed, etc.): *i*) a control simulation using atmospheric forcing of present day conditions $\psi_{Control} = \psi_{NCEP}$, where ψ_{NCEP} is the National Centers for Environmental Prediction (NCEP)/National Center for Atmospheric Research (NCAR) reanalyzed atmospheric forcing (43) (56 years, from 1948 to 2004) applied to the 2005–2061 period; and *ii*) a GW simulation that makes use of an atmospheric forcing for a GW scenario $\psi_{GW} = \psi_{Control} + \psi^*_{IPSL}$, where ψ^*_{IPSL} are the atmospheric forcing anomalies from the IPSL (Institut Pierre-Simone Laplace) earth system model simulation based on an Intergovernmental Panel on Climate Change scenario A2 (44). Thus, ψ^*_{IPSL} is the difference between the atmospheric output variables from a climate IPSL-A2 run with increasing CO_2 (56 years, from ≈ 377 ppm in 2005 to ≈ 551 ppm in 2061) and the baseline of 30-year monthly averages (into 1-year climatology, from 1974 to 2004) of the same simulation. Each monthly value of the ψ^*_{IPSL} anomalies was smoothed with a running-mean of 30 years to remove interannual variability while maintaining the seasonality (15).

Thus, we obtained estimates of the MLD and CHL under GW (MLD^{GW} and CHL^{GW}; $\approx 50\%$ increase in CO_2 with respect to 2005 levels) as well as without GW (MLD^{Control} and CHL^{Control}) (15). By applying both the SRD-model and the MLD-model we next obtained, for each model, a DMS concentration estimates for the GW scenario (DMS$^{GW}_{model}$) and the control (DMS$^{Control}_{model}$). For the SRD-model, surface solar irradiance and the light extinction coefficient were assumed to remain the same in both scenarios, so that DMS changes will only be the result of the differences between MLD^{GW} and MLD^{Control}, which translate into differences between SRD^{GW} and SRD^{Control}. When the MLD-model is used, either changes in MLD and CHL may result in DMS differences. The SRD-model equation does not include CHL; therefore, it cannot capture changes in the bloom-regime regions due to GW, but rather only changes in the stress-regime regions (11). On the other hand, the MLD-model has two empirical equations, one of which includes both MLD and CHL (to be used in bloom-regime regions), whereas the other estimates DMS exclusively as a function of the MLD (to be used in stress-regime regions) (3, 7). Therefore, the MLD-model is expected to account for changes in both regime regions. Never-

theless, for either the GW or Control scenarios, the stress-regime clearly dominated, and DMS was estimated solely from the MLD in ≈90% of the ocean's surface.

Global Maps of Averaged DMS Increase Due to Global Warming. By comparing the global maps of DMS obtained for the GW and Control scenarios, we calculated the DMS change due to GW (the change in the absolute value and the percentage of change) for every $1° \times 1°$ grid box (or pixel) of the global ocean. These estimates were obtained for three periods separately: annually, from April to September, and from October to March. The changes in the absolute value (nM) were obtained as follows:

$$\Delta DMS_{\text{Annual}} = \frac{1}{12} \left(\sum_{i=\text{Jan}}^{i=\text{Dec}} DMS_i^{GW} \Delta t - \sum_{i=\text{Jan}}^{i=\text{Dec}} DMS_i^{\text{Control}} \Delta t \right)$$

[5]

$$\Delta DMS_{\text{Apr-Sep}} = \frac{1}{6} \left(\sum_{i=\text{Apr}}^{i=\text{Sep}} DMS_i^{GW} \Delta t - \sum_{i=\text{Apr}}^{i=\text{Sep}} DMS_i^{\text{Control}} \Delta t \right)$$

[6]

$$\Delta DMS_{\text{Oct-Mar}} = \frac{1}{6} \left(\sum_{i=\text{Oct}}^{i=\text{Mar}} DMS_i^{GW} \Delta t - \sum_{i=\text{Oct}}^{i=\text{Mar}} DMS_i^{\text{Control}} \Delta t \right),$$

[7]

where Δt is 1 month. The percentages of DMS change were calculated by normalizing the absolute changes by the annual mean concentration of the Control scenario:

$$\Delta DMS_k^\% = \frac{\Delta DMS_k}{\frac{1}{12} \sum_{i=\text{Jan}}^{i=\text{Dec}} DMS_i^{\text{Control}} \Delta t} \times 100,$$

[8]

where DMS_k can be DMS_{Annual}, $DMS_{\text{Apr-Sep}}$, or $DMS_{\text{Oct-Mar}}$.

Globally Averaged DMS Increase Due to Global Warming. Following a similar procedure, by considering the DMS change in each month and pixel along with the area covered by the pixel, the globally averaged (not spatially resolved) percentage of DMS change due to GW was obtained for three cases: annually and summer and winter conditions. By summer and winter conditions, we mean the regions and periods with a daily averaged solar surface irradiance higher and lower than 200 W m^{-2}, respectively.

1. Charlson RJ, Lovelock JE, Andreae MO, Warren SG (1987) *Nature* 326:655–661.
2. Simó R, Pedros-Allió C (1999) *Nature* 402:396–399.
3. Simó R, Dachs J (2002) *Global Biogeochem Cycles* 16, 10.1029/2001GB001829.
4. Wolfe GV, Strom SL, Holmes JL, Radzio T, Olson MB (2002) *J Phycol* 38:948–960.
5. Sunda W, Kleber DJ, Kiene RP, Huntsman S (2002) *Nature* 418:317–320.
6. Slezak D, Herndl GJ (2003) *Mar Ecol Prog Ser* 246:61–71.
7. Toole DA, Siegel DA (2004) *Geophys Res Lett* 31, 10.1029/2004GL019581.
8. Toole DA, Slezak D, Kiene RP, Kieber DJ, Siegel DA (2006) *Deep Sea Res I* 53:136–153.
9. Hefu Y, Kirst GO (1997) *Polar Biol* 18:402–409.
10. Stefels J, van Leeuwe MA (1998) *J Phycol* 34:486–495.
11. Vallina SM, Simó R (2007) *Science* 315, 506–508.
12. Vallina SM, Simó R, Gassó S, de Boyer-Montégut C, del Río E, Jurado E, Dachs J (2007) *Global Biogeochem Cycles* 21:GB2004.
13. Vallina SM, Simó R, Gassó S (2006) *Global Biogeochem Cycles* 20:GB1014.
14. Aranami K, Tsunogai S (2004) *J Geophys Res* 109:D12303.
15. Manizza M (2006) PhD thesis (University of East Anglia, Norwich, UK).
16. Prospero JM, Savoie DL, Saltzman ES, Larsen R (1991) *Nature* 350:221–223.
17. Ayers G, Gras JL (1991) *Nature* 352:834–835.
18. Andreae MO, Elbert W, de Mora SJ (1995) *J Geophys Res* 100:11335–11356.
19. Ayers GP, Cainey JM, Gillett RW, Ivey JP (1997) *Philos Trans R Soc London B* 352:203–211.
20. Clarke AD, Davis D, Kapustin VN, Eisele F, Chen G, Paluch I, Lenschow D, Bandy AR, Thornton D, Moore K, et al. (1998) *Science* 282:89–92.
21. Andreae MO, Elbert W, Cai Y, Andreae TW (1999) *J Geophys Res* 104:21695–21706.
22. Ayers G, Gillett RW (2000) *J Sea Res* 43:275–286.
23. Gunson JR, Spall SA, Anderson TR, Jones A, Totterdell IJ, Woodage MJ (2006) *Geophys Res Lett* 33:L07701.
24. Kettle AJ, Andreae MO (2000) *J Geophys Res* 105(D22):26793–26808.
25. Meehl GA (1987) *Geographical J* 153:21–36.
26. Miller AJ, Alexander MA, Boer GJ, Chai F, Denman K, Erickson DJ, III, Frouin R, Gabric AJ, Laws EA, Lui Z, et al. (2003) *Bull Am Meteorol Soc* 84:617–633.
27. Hynes AJ, Wine PH, Semmes DH (1986) *J Phys Chem* 90:4148- 4156.
28. Spivakovsky CM, Logan JA, Montzka SA, Balkanski YJ, Foreman-Fowler M, Jones DBA, Horowitz LW, Fusco AC, Brenninkmeijer CAM, Prather MJ, et al. (2000) *J Geophys Res* 105:8931–8980.
29. Stark H, Brown SS, Goldan PD, Aldener M, Kuster WC, Jakoubek R, Fehsenfeld FC, Meagher J, Bates TS, Ravishankara AR (2007) *J Geophys Res* 112:D10S10.
30. Bopp L, Boucher O, Aumont O, Belviso S, Dufresne JL, Pham M, Monfray P (2004) *Can J Fish Aquat Sci* 61:826–835.
31. Gabric AJ, Simó R, Cropp RA, Hirst AC, Dachs J (2004) *Global Biogeochem Cycles* 18:GB2014.
32. Andreae MO, Crutzen PJ (1997) *Science* 276:1052–1058.
33. van Rijssel M, Gieskes WWC (2002) *J Sea Res* 48:17–27.
34. Timmermann R, Goosse H, Madec G, Fichefet T, Ethe C, Duliere V (2005) *Ocean Modelling* 8:175–201.
35. Madec G, Imbard M (1996) *Clim Dyn* 12:381–388.
36. Madec G, Delecluse P, Imbard M, Lévy C (1999) *Ocean General Circulation Model Reference Manual* (Lab d'Océanogr Dyn et de Climatol, Paris), OPA 8.1.
37. Gaspar P, Gregoris Y, Lefevre JM (1990) *J Geophys Res* 95:16179–16193.
38. Gent PR, McWilliams JC (1990) *J Phys Oceanogr* 20:150–155.
39. LeQuéré C, Harrison SP, Prentice IC, Buitenhuis ET, Aumont O, Bopp L, Claustre H, da Cunha LC, Geider R, Giraud X, et al. (2005) *Global Change Biol* 11:2016–2040.
40. Kiehl JT, Trenberth E (1997) *Bull Am Meteorol Soc* 78:197–208.
41. Brock TD (1981) *Ecol Modelling* 14:1–19.
42. Smith RC, Baker KS (1979) *Photochem Photobiol* 29:311–323.
43. Kistler R, Kalnay E, Collins W, Saha S, White G, Woollen J, Chelliah M, Ebisuzaki W, Kanamitsu M, Kousky V, et al. (2001) *Bull Am Meteorol Soc* 82:247–267.
44. Friedlingstein P, Bopp L, Ciais P, Dufresne, J-L, Fairhead L, LeTreut H, Monfray P, Orr J (2001) *Geophys Res Lett* 28:1543–1546.
45. de Boyer-Montégut C, Madec G, Fischer AS, Lazar A, Iudicone D (2004) *J Geophys Res* 109:C12003.
46. Gabric AJ, Whetton PH, Cropp R (2001) *Tellus Ser B* 53:273–287.
47. Vila-Costa M, Kiene RP, Simó R (2007) *Limnol Oceanogr*, in press.

ENVIRONMENTAL SCIENCES